Macromolecular Chemistry and Physics
www.mcp-journal.de

Glycidyl Cinnamate: Copolymerization with Glycidyl Ethers, In-Situ NMR Kinetics, and Photocrosslinking

*Kamil Maciol, Sandra Schüttner, Jan Blankenburg, Tobias Johann, and Holger Frey**

The copolymerization of glycidyl cinnamate (GC) as a hitherto non-polymerizable, photoreactive epoxide structure to aliphatic polyether copolymers is described, using the monomer-activated epoxide ring-opening polymerization (MAROP). Ethoxyethyl glycidyl ether (EEGE) and GC are copolymerized employing triisobutylaluminum (*i*-Bu_3Al) as a catalyst and tetraoctylammonium bromide ($NOctBr_4$) as an initiator. The amount of GC varies from 3 mol% to 100 mol%, which results in apparent molecular weights in the range of 2600 to 4600 g mol^{-1} and dispersities (*Đ*) below 1.34. Studies of the microstructure by in-situ ^{1}H NMR kinetics indicate a gradient-like distribution of EEGE and GC (reactivity ratios: $r_{EEGE} = 0.28$; $r_{GC} = 3.6$), applying the ideal copolymerization model for evaluation. A tentative explanation relies on differing bond lengths in the respective epoxide rings, as suggested by density functional theory (DFT) calculations. Mild and selective cleavage of the acetal protecting groups of EEGE is achieved using the acidic ionic resin Dowex, leaving the GC ester bonds intact (M_n = 1900–3700 g mol^{-1}, $Đ < 1.34$). Thermal properties of the copolymers and the PGC homopolymer are investigated by differential scanning calorimetry (DSC). The crosslinking of P(G-*co*-GC) copolymers by UV irradiation allows hydrogel formation, which is confirmed by IR spectroscopy.

1. Introduction

Crosslinkable polymer structures for thermosets or composites often rely on acrylates and methacrylates.[1] In recent work photoreversible hydrogels were described, derived from coumarin-containing polyacrylates.[2] However, polyether structures bearing reactive or polymerizable monomer units have only been studied to a very limited extent. In this context, glycidyl esters represent a very interesting platform to generate photocrosslinked polymer networks. Glycidyl esters with a variety of substituents are known.[3] This class of compounds has hardly been explored to date with respect to ring-opening polymerization due to the harsh, basic conditions of the conventional oxyanionic polymerization,[4] which lead to saponification of the glycidyl esters. Consequently, one has to resort to other polymerization mechanisms, such as the monomer-activated ring-opening polymerization (MAROP), pioneered by Carlotti and Deffieux[5,6,7a–c,8,9] with the polymerization of glycidyl methacrylate (GMA).[10] In 2020, our group extended the library of ester functional polyethers via MAROP. The copolymerization of ethylene oxide (EO) with the tailor-made ester functional epoxides methyl 4,5-epoxypentenoate (MEP) and ^{t}butyl 4,5-epoxypentenoate (^{t}BEP) was reported and also provided access to novel carboxylic acid functional poly(ethylene glycol) (PEG) copolymers after cleavage of the ester protective groups.[11] Further, Kim and coworkers applied a glycidyl ether analogue, *t*-butyl glycidoxy acetate (tBGA) in a MAROP. Acidic hydrolysis leads to poly(glycidoxy acetic acid) (PGA), comprising H-bonding donor and acceptor moieties within one monomer repeating unit.[12] Alternatively, these polymer architectures are also accessible by coordination–insertion polymerization, however, this results in broader molar mass distributions.[13]

Glycidyl cinnamate (GC) is the glycidyl ester of cinnamic acid and possesses both a reactive double bond and an epoxide function.[14,15] Cinnamic acid is an intermediate metabolite in the lignin-biosynthesis process and hence represents a biosourced monomer precursor.[16] As a photocrosslinkable monomer, the glycidyl ester of cinnamic acid is of particular interest, because it represents a bifunctional monomer. GC possesses a polymerizable epoxide moiety and a photosensitive cinnamoyl group. Cinnamic acid derivatives undergo a [2+ 2] photocycloaddition, isomerization or a photo-Fries rearrangement under UV irradiation.[17a–c,18] Previous access to the cinnamoyl groups in polyethers was achieved by post-polymerization modification, since the harsh conditions of an AROP would cleave the ester

K. Maciol, S. Schüttner, J. Blankenburg, T. Johann, H. Frey
Institute of Organic Chemistry
Johannes Gutenberg University Mainz
Duesbergweg 10–14, 55128 Mainz, Germany
E-mail: hfrey@uni-mainz.de
J. Blankenburg
Graduate School Materials Science in Mainz
Staudinger Weg 9, 55128 Mainz, Germany
T. Johann
Max Planck Graduate Center with the Johannes Gutenberg University
Staudinger Weg 6, 55128 Mainz, Germany

The ORCID identification number(s) for the author(s) of this article can be found under https://doi.org/10.1002/macp.202200366

DOI: 10.1002/macp.202200366

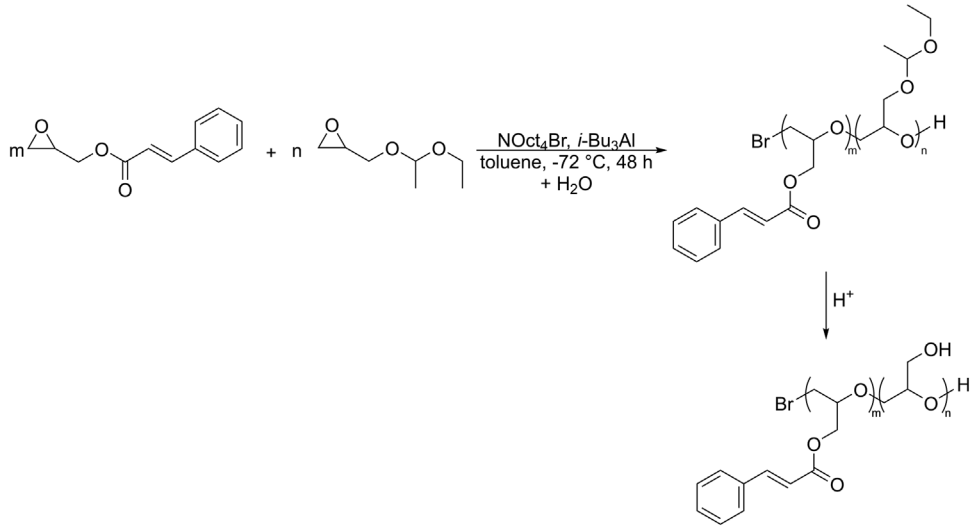

Scheme 1. Synthesis of P(G-*co*-GC) via the monomer activation technique by copolymerization of EEGE and GC and subsequent acidic cleavage of the protecting groups.

structure. Trzebicka et al. modified linear poly(ethylene oxide)-*b*-polyglycerol *lin*P(EO-*b*-G) block copolymers using cinnamic acid to nanogels synthesized by UV irradiation.[19] The photoreactivity of the cinnamic acid moiety was already used in various photoresponsive polymer structures like polyvinyl cinnamic acid ester (PVCm), which was the first synthesized photopolymer to be used as a negative-tone photoresist.[18,20,21] Application for drug delivery systems was demonstrated by Shi et al. with the synthesis of degradable, photoresponsive nanoparticles. Starting from 3,4-dihydroxycinnamic acid (3,4DHCA), 4-hydroxycinnamic acid (4HCA) and dithiothreitol (DTT), photoresponsive PCA-*graft*-DTT nanoparticles were prepared, in which protein encapsulation was achieved during nanoparticle formation.[22] Recently, Zhao et al. synthesized an acrylated, acid-degradable PEG hydrogel with a single cinnamaldehyde acetal unit in the initiator system. However, thiol-ene click reaction was performed under basic conditions to prevent crosslinking by the degradable cinnamaldehyde acetal unit.[23] Polyglycerol (PG) represents a highly biocompatible and hydrophilic material.[24] Both linear and branched PG are water-soluble, showing structural similarity to PEG, but possess functional groups at the polyether backbone.[25] The direct anionic ROP (AROP) of glycidol is not applicable for the synthesis of linear PG (*lin*PG) due to the inimer (initiator–monomer) structure of glycidol, which leads to branching.[26] The use of suitable protecting groups allows for the formation of linear polyether structures. Ethoxyethyl glycidyl ether (EEGE)[27] is commonly applied for the synthesis of *lin*PG, capitalizing on the acetal moiety as a base-stable protecting group.[28] Each hydroxyl group of *lin*PG offers an anchor point for the introduction of various functional groups by post-polymerization modification, which renders the polymer attractive for biomedical application.[29] Potential applications for *lin*PG include the use for drug delivery systems or bioconjugation with proteins ("PGylation"),[30] coatings for gold surfaces,[31] or star-shaped macroinitiators for star block copolymers with core–shell structure.[25,32]

In this work, we describe the statistical copolymerization of EEGE and GC. To the best of our knowledge, the anionic polymerization of GC has not been described to date. Obviously, conventional AROP is not applicable for the polymerization of GC, since cleavage of the ester moiety cannot be avoided under basic reaction conditions. Furthermore, a chain transfer reaction to the monomer caused by the proton abstraction from the methylene proton adjacent to the epoxide ring is a weight limiting side reaction for substituted epoxides.[33] However, employing the MAROP, *lin*P(G-*co*-GC) copolymers have been synthesized under mild conditions, circumventing saponification of the ester and proton abstraction.[5,6,8,9] **Scheme 1** shows the synthetic strategy for the copolymerization of EEGE and GC. The copolymers were characterized taking into account the selective cleavage of the acetal groups of EEGE as well as thermal properties and microstructure of the copolymers. In addition, photocrosslinking of cinnamate-containing P(G-*co*-GC) copolymers without additives were studied and hydrogels formed.

2. Results and Discussion

2.1. Synthesis of the GC Monomer

The preparation of glycidyl cinnamate was performed by esterification of epichlorohydrin with cinnamic acid, which was converted into an activated nucleophile with KOH. It should be emphasized that compared to literature, the yield could be increased by ≈17%, which is due to a higher amount of phase transfer catalyst and longer reaction times.[14] In general, GC is readily storable in the refrigerator (4 °C) with high storage stability. Temperatures of 150 °C and a pressure of 1×10^{-3} mbar are required for monomer distillation. For the corresponding ^{1}H NMR, ^{13}C NMR, and 2D NMR spectra, see Figures S1–S4, Supporting Information.

2.2. Copolymerization of EEGE and GC

The synthesis of the copolymers was performed employing an initiator/catalyst system consisting of tetraoctylammonium

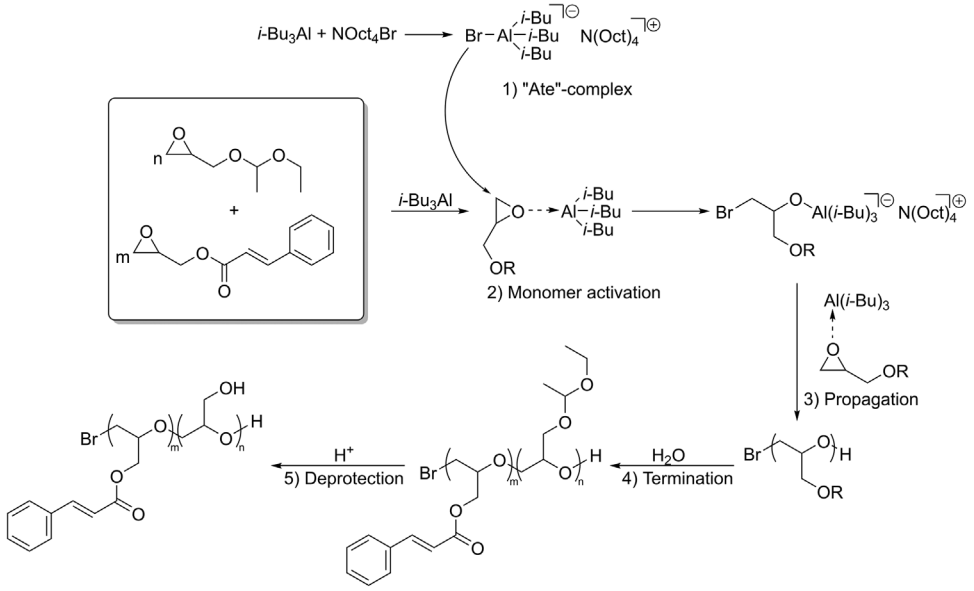

Scheme 2. Reaction mechanism for the copolymerization of EEGE and GC initiated by $NOct_4Br$: i) formation of the "ate"-complex; ii) activation of the monomers by complexation and nucleophilic attack of bromide; iii) chain growth; iv) termination by addition of water; and v) acidic cleavage of the acetals.

Table 1. Copolymerization of EEGE with GC using [i-Bu_3Al]/[$NOct_4Br$] as a catalyst–initiator system (synthesis in toluene, −72 °C).

No.	Copolymer composition[a)]	Theoretical composition EEGE:GC [a),b),d)]	$M_n^{(th)}$ [c)] [g mol^{-1}]	M_n [d)] [g mol^{-1}]	$Đ$ [d)]	[i-Bu_3Al]/[$NOct_4Br$] [e)]
1	PGC	0:100	10 000	2600	1.19	4.5
2	P($EEGE_{0.17}$-*co*-$GC_{0.83}$)	19:81	10 000	2200	1.20	4.5
3	P($EEGE_{0.27}$-*co*-$GC_{0.73}$)	30:70	10 100	2300	1.34	5.0
4	P($EEGE_{0.70}$-*co*-$GC_{0.30}$)	69:31	10 200	4600	1.21	4.5
5	P($EEGE_{0.81}$-*co*-$GC_{0.19}$)	80:20	10 100	3800	1.19	4.5
6	P($EEGE_{0.84}$-*co*-$GC_{0.16}$)	85:15	10 100	3400	1.09	5.0
7	P($EEGE_{0.92}$-*co*-$GC_{0.08}$)	92:8	10 700	4500	1.28	5.0
8	P($EEGE_{0.97}$-*co*-$GC_{0.03}$)	96:4	10 100	4400	1.11	5.0

[a)] Obtained from ^{1}H NMR spectra; [b)] The theoretical composition refers to the calculated $M_n^{(th)}$ in column 3; [c)] $M_n^{(th)}$ was calculated via the [monomer]/[initiator] ratio; [d)] Determined by SEC measurements in DMF (RI detector, PEG standards); [e)] Catalyst/initiator ratio.

bromide ($NOct_4Br$) as an initiator and triisobutylaluminum i-Bu_3Al as a catalyst. The catalyst was used in excess (**Scheme 2**),[9] because i-Bu_3Al acts simultaneously as a monomer activator in addition to forming an "ate"-complex with $NOct_4Br$. Since the initiator/catalyst ratio influences the propagation rate and molecular weight distributions, the ratio has to be adjusted specifically for each monomer system. Full removal of the catalyst and the hydrolyzed initiator residues represents a critical issue. There are different approaches in literature.[34] In our work, by termination with Milli-Q water, i-Bu_3Al was transformed into the amphoteric aluminum hydroxide and removed by filtration. Subsequent dialysis in dichloromethane/methanol (3:2) removed the residues of the initiator.

Table 1 summarizes the data obtained by size exclusion chromatography (SEC) (RI detector, DMF, PEG standards) for the series of copolymers prepared with GC. Molar masses between 2200 and 4600 g mol^{-1} were obtained with dispersities ($Đ$) between 1.09 and 1.34. The SEC traces of all P(EEGE-*co*-GC) copolymers and the PGC homopolymer (**Figure 1**; Figure S5, Supporting Information) display monomodal molecular weight distributions. GC was incorporated in any desired ratio. All batches targeted molecular weights of 10 000 g mol^{-1}. The primary reason for the discrepancies seen in the molecular weights is the SEC calibration, carried out using PEG standards, which only provides exact values for pure PEG. This finding is substantiated by a comparison with the literature. Schömer et al. targeted a PEEGE homopolymer of 7500 g mol^{-1} and measured 2700 g mol^{-1} despite full monomer conversion.[35] A similar discrepancy of about 60% between the theoretical and molecular weight determined by SEC can be observed for sample P($EEGE_{0.97}$-*co*-$GC_{0.03}$) (entry 8, Table 1), which shows the lowest content of GC and features the most similar structure to a PEEGE homopolymer. In general, the molecular weight deviation increases with the amount of GC incorporated in the copolymers, since the

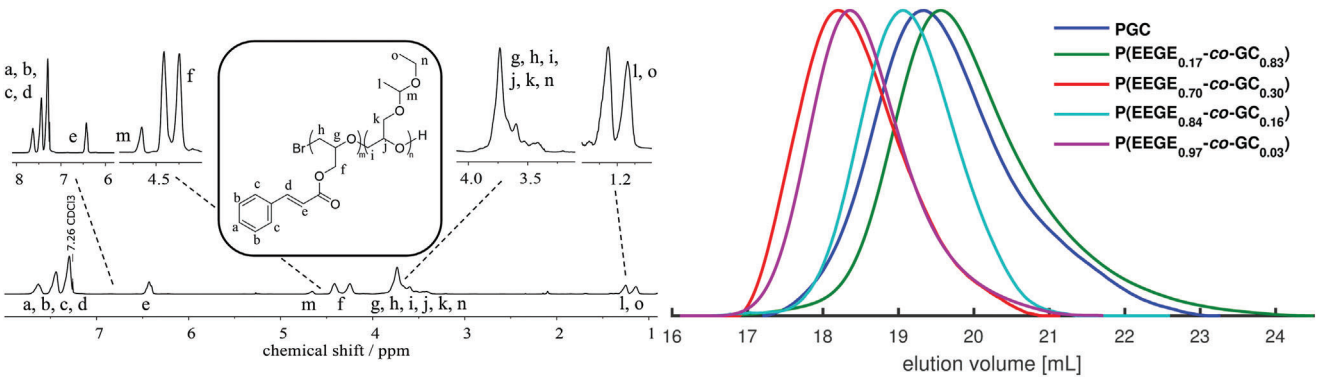

Figure 1. ^{1}H NMR spectrum (600 MHz, $CDCl_3$) of P(EEGE$_{0.84}$-*co*-GC$_{0.16}$) (entry 6, Table 1) and SEC traces (RI detector, DMF, PEG standards) of selected P(EEGE-*co*-GC) copolymers and PGC homopolymer.

hydrodynamic radius of the copolymers differs to an increasing extent from that of the PEG standards. PEEGE and PGC both represent substituted hydrophobic polyethers, which cause a change of the hydrodynamic radius of the copolymer coils to a varying extent. The overlap of RI and UV signal proves homogeneous incorporation of GC and EEGE over the entire molecular weight distribution of the copolymers (Figure S6, Supporting Information).

Due to the absence of a functional initiator, solely the incorporation ratios can be determined via ^{1}H NMR, but no absolute molecular weights are accessible. MALDI-ToF characterization (Figure S7, Supporting Information) for P(EEGE$_{0.97}$-*co*-GC$_{0.03}$) (entry 8) does not only verify the bromide-initiated synthesis of the copolymers, but also demonstrates that molecular weights of at least 8400 g mol^{-1} were achieved (MALDI-ToF is known for its mass discrimination effects).[36]

Monomer incorporation was in agreement with the monomer ratios employed (Table 1). Characteristic signals at 6.4 ppm (proton of GC double bond) and 4.7 ppm (methine proton of EEGE) from the ^{1}H NMR spectrum (Figure 1) were used for the evaluation. Additional inverse gated ^{13}C NMR and 2D NMR spectra are provided in Figures S8–S10, Supporting Information. As the monomer-activated monomer polymerization technique is well-known for the suppression of the chain transfer reaction under basic conditions (Figure S11, Supporting Information), the absence of allyl-initiated polymer chains in ^{1}H NMR analysis confirms the controlled copolymerization of EEGE and GC.[33,37]

The last column of Table 1 indicates the catalyst/initiator ratio, which had to be adjusted for each copolymerization with different monomer ratios to provide optimal reaction conditions. For propylene oxide (PO), Carlotti et al. already showed that high catalyst–initiator ratios caused broadening of the molecular weight distributions and that no polymerization took place at a ratio ≤1.[5,38] The amount of catalyst must be chosen according to the structure of the comonomers and EEGE exhibits a strong coordination capability with the catalyst. In general, increasing oxygen content in the monomer structure requires higher amounts of catalyst for the copolymerization due to interaction and complexation of the aluminum catalyst (Figure S12, Supporting Information).[9]

2.3. In-Situ ^{1}H NMR Kinetics

In-situ ^{1}H NMR spectroscopy has become an established method for the investigation of monomer gradients in living copolymerizations. We recently employed in-situ NMR studies for the monomer-activated AROP to elucidate the microstructure of the resulting copolymers.[39,40] This method is advantageous, since the copolymerization takes place undisturbed in the NMR tube without manual sample removal, avoiding an external manipulation. In this manner, possible contamination by traces of oxygen or water is avoided. In addition, the safety aspect is not negligible, since *i*-Bu$_3$Al is pyrophoric and reacts violently in air. In the case of copolymerization with the gaseous, toxic, carcinogenic and mutagenic EO, this technique can also prevent possible contamination of the environment by undissolved gas, which can occur when withdrawing samples for kinetic studies.[41] In a previous work, we published the reaction kinetics of EO with the glycidyl esters MEP and ^{t}BEP via MAROP, resulting in a random and gradient structure, respectively.[11] To the best of our knowledge, the reaction kinetics of glycidyl esters with glycidyl ethers has not been investigated to date via real-time ^{1}H NMR spectroscopy. The monomer distribution in copolymers is highly dependent on the chemical nature of the monomers for the monomer-activated anionic ring-opening copolymerization. The copolymerization of different glycidyl ethers results in a random monomer sequence,[40,42] while the copolymerization of EO and glycidyl ethers provides strongly tapered copolymer structures with a preferred incorporation of EO in case of monomer activation by *i*-Bu$_3$Al.[39] The same applies to the copolymerization of glycidyl ethers and propylene oxide (PO), which behaves similar to EO in this case.[9] Comparing the reactivity ratios of EO and PO, a higher reactivity of EO can be observed.[38]

Relying on the integrals of the signals for the proton of the GC double bond (6.4 ppm) and the methylene protons of EEGE (3.1 ppm), the decrease of the monomer concentrations was monitored (**Figure 2**) via in-situ ^{1}H NMR kinetics at −20 °C in toluene-d_8. Although the polymerization temperature impacts the copolymerization rates, the reactivity ratios remain independent of temperature.[35,43] Thus, the selection of a copolymerization temperature of −20 °C was expected to result in a suitable reaction rate for NMR kinetics. The SEC trace of the resulting

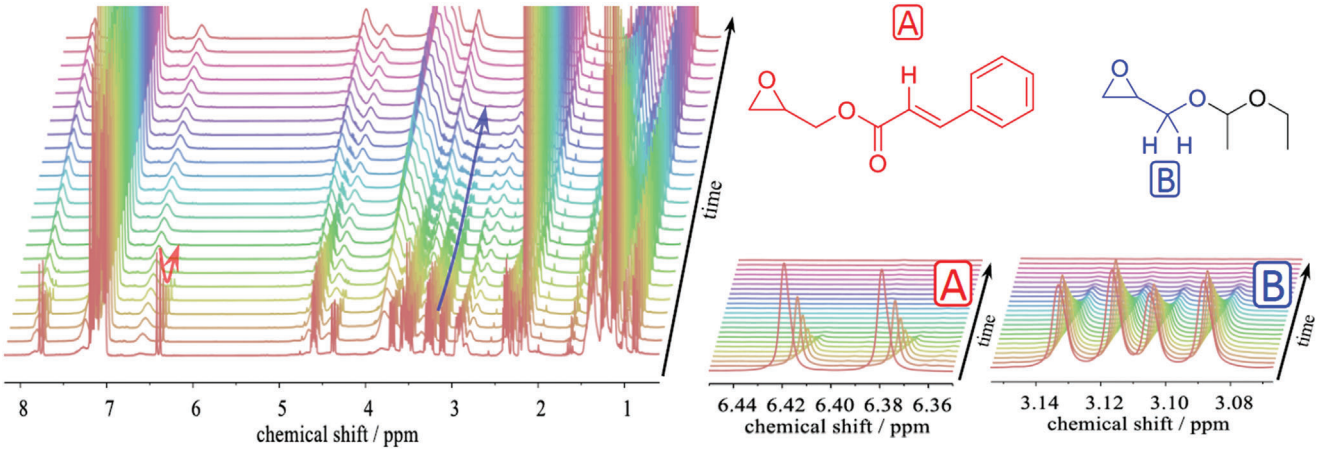

Figure 2. ^{1}H NMR spectra for the copolymerization of EEGE and GC in toluene-d_8 at −20 °C, monomer activation method; right: zoom-in of relevant areas of the spectrum for evaluation.

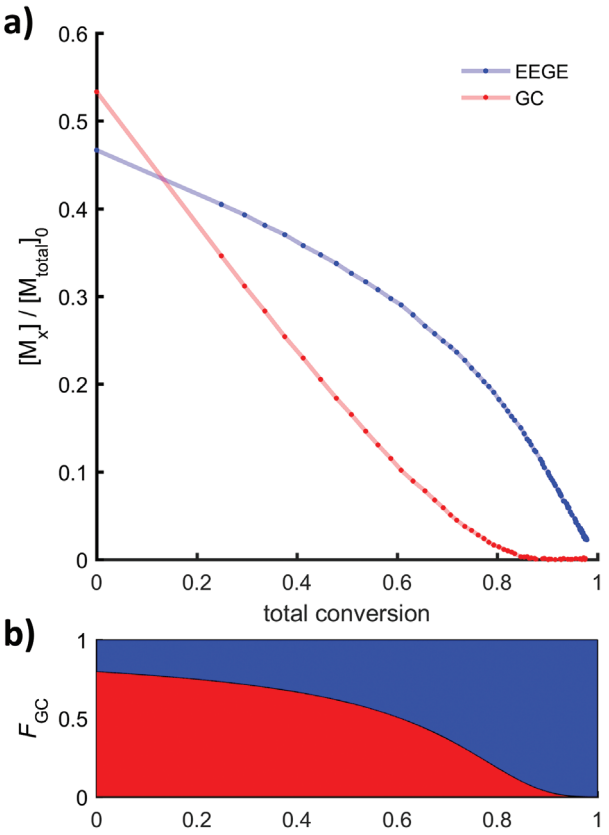

Figure 3. Top a): monomer concentration plotted versus total monomer conversion determined by ^{1}H NMR spectroscopy in toluene-d_8 at −20 °C, applying the monomer-activated AROP. Blue line: conversion of EEGE, red line: conversion of GC. Bottom b): calculated P(EEGE-*co*-GC) microstructure based on the reactivity ratios determined from the ideal model (ideal integrated equation).[44]

copolymer demonstrates the successful copolymerization (Figure S13, Supporting Information). The decrease of the monomer signals can be directly translated to their incorporation into the copolymer chains formed, since no transfer or termination reactions occur. **Figure 3**a illustrates the concentration of EEGE and GC plotted versus total conversion, indicating a gradient structure of the copolymers.

Table 2. Reactivity ratios for the monomer-activated ring opening copolymerization of EEGE and GC in toluene at −20 °C, initiated with $NOct_4Br$ and i-Bu_3Al as catalyst.

Method	r_{EEGE}	r_{GC}
Ideal-Integrated	0.28	3.6
Jaacks	0.25	3.9
Meyer–Lowry	0.16	2.7

The data obtained by the in-situ measurement can be fitted by various copolymerization models to obtain reactivity ratios. For Wall's[45] copolymerization model (ideal/non-terminal) the ideal-integrated method[44] and Jaacks[46] method was used. For the fit of the Mayo–Lewis[47] model (terminal) the Meyer–Lowry[48] equation was used (**Table 2**).

The corresponding fits are supplied in Figures S14–S16, Supporting Information. All methods provide similar reactivity ratios and demonstrate the preferred incorporation of GC. Our group has shown in the past that fits using the more-complex Mayo–Lewis model can lead to overfitting.[49] For this reason, we use the reactivity ratios by the less error-prone ideal model for the calculation of the copolymer microstructure. Based on the reactivity ratios determined by the ideal-integrated equation, the average comonomer composition along the polymer chains can be calculated.[50] The result is shown in Figure 3b, revealing a gradient-like microstructure. The resulting copolymerization diagram is depicted in Figure S17, Supporting Information. The reactivity ratios observed are consistent with work by Labbé et al. who demonstrated that glycidyl methacrylate (GMA) incorporates faster than glycidyl methyl ether (GME) (r_{GME} = 0.37; r_{GMA} = 1.24).[10]

As an explanation for the EEGE/GC reactivity ratios, steric influence can be ruled out, since GC is incorporated preferentially, despite the bulky side group. Instead, the pronounced gradient must be a result of the chemical nature of the monomers. To

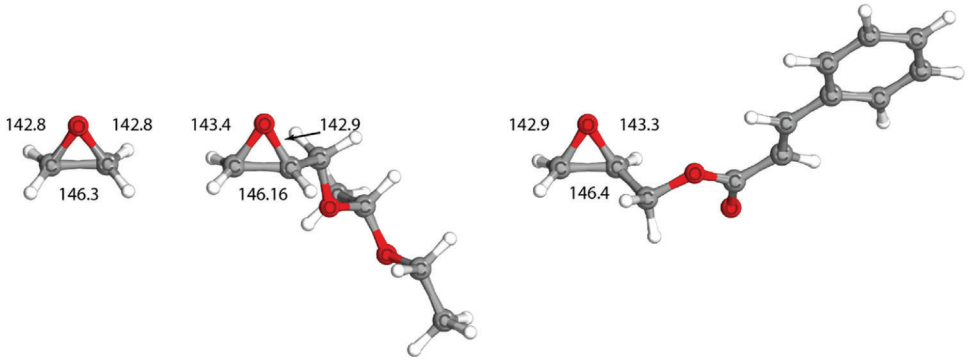

Figure 4. Determined bond lengths (in picometers) for EO, EEGE, and GC via DFT calculations.

correlate the reactivity ratios to the molecular structure of EEGE and GC, quantum mechanical calculations (B3LYP-D3-gCP/def2-TZVP//B3LYP-D3-gCP/def2-TZVP) were performed. As a simplified model, the bond length of the epoxide C–O bond, which is attacked during propagation to form the backbone (for coordinates, see Tables S1–S3, Supporting Information), was investigated. In the case of EEGE, this bond is slightly longer (143.4 pm) compared to GC (142.9 pm) or EO (142.8 pm). This leads to an increased ring strain toward the site for nucleophilic attack in GC compared to EEGE. Furthermore, the bond lengths in EO and GC show only slight differences, thus similar ring strain and reactivity can be expected. In a previous report by our group, a pronounced gradient was observed for EO and EEGE, when copolymerized via monomer-activated AROP (r_{EO} = 8.00; r_{EEGE} = 0.125).[39] From the calculated ring geometries, GC can be expected to show similar reactivity as EO (**Figure 4**), which is considerably more reactive in the monomer-activated copolymerization than EEGE. This is in line with our findings regarding gradient type copolymerization of EEGE and GC.

2.4. Removal of the Acetal Protective Groups to Release Hydroxyl Groups

Cleavage of the acetal group subsequent to the polymerization without affecting the GC ester bonds is not trivial. For this purpose, the acidic ion exchange resin Dowex 50WX8 was used for deprotection. Quantitative removal of the protective groups was achieved using a methanol/toluene mixture and reduced pressure. Continuous removal of the cleavage products acetaldehyde and ethanol resulted in shifting of the reaction equilibrium toward the product side. Consequently, a drastic difference in the polarity of the polymer samples could be observed. While all the protected samples of Table 1 were only soluble in organic solvents such as dichloromethane, the deprotected samples 11–15 (**Table 3**) could be dissolved in water, which is crucial for the preparation of hydrogels, as discussed below. Table 3 gives the SEC data for all deprotected P(G-*co*-GC) copolymers. Apparent molecular weights are in the range of 1900 to 3700 g mol^{-1} with $Đ$ below 1.35.

A superposition of selected SEC traces of P(G-*co*-GC) copolymers is shown in **Figure 5** and demonstrates the monomodal distributions obtained. In direct comparison, all individual elugrams are shifted to higher elution volumes (lower molecular weights), when compared to the protected precursors. Successful deprotection is also evidenced by the ^{1}H NMR spectrum, shown for the deprotected P($G_{0.18}$-*co*-$GC_{0.82}$) copolymer (entry 9, Table 3) in Figure 5. The typical signals of the acetal protecting group at 4.7 ppm and 1.2 ppm are absent, confirming quantitative cleavage. In addition, all characteristic signals of glycidyl cinnamate are still present. The Supporting Information includes additional ^{13}C NMR and 2D NMR spectra (Figures S18–S20, Supporting Information) and additional SEC curves of deprotected copolymers (Figure S21, Supporting Information, entries 10,12,14 in Table 3).

Table 3. Characterization data of deprotected polyglycerol copolymers.

No.[a]	Copolymer composition[b]	Theoretical composition	M_n (th) [g mol^{-1}]	M_n[c] [g mol^{-1}]	$Đ$[c]
9(2)	P($G_{0.18}$-co-$GC_{0.82}$)	19:81	9300	1900	1.25
10(3)	P($G_{0.29}$-co-$GC_{0.71}$)	30:70	8900	2200	1.33
11(4)	P($G_{0.70}$-co-$GC_{0.30}$)	69:31	7100	3500	1.32
12(5)	P($G_{0.81}$-co-$GC_{0.19}$)	80:20	6400	3700	1.21
13(6)	P($G_{0.86}$-co-$GC_{0.14}$)	85:15	6100	2400	1.30
14(7)	P($G_{0.92}$-*co*-$GC_{0.08}$)	92:8	6000	3300	1.34
15(8)	P($G_{0.98}$-co-$GC_{0.02}$)	96:4	5400	3600	1.21

[a] Exponent specifies precursor from Table 1; [b] Obtained from ^{1}H NMR spectra; [c] Determined by SEC measurements in DMF (RI detector, PEG standards).

2.5. Thermal Characterization of the Copolymers

Thermal properties of the copolymers were investigated by differential scanning calorimetry (DSC). **Table 4** documents the thermal characteristics for both P(EEGE-*co*-GC) and the deprotected P(G-*co*-GC) copolymers as well as PGC homopolymer. All values were determined from the second heating curve (for DSC diagrams see Figures S22 and S23, Supporting Information). The glass transition temperatures (T_gs) vary in the range of −60 °C (entry 8, Table 4) for protected copolymers and −13 °C (entry 15, Table 4) after deprotection, to 21 °C (entry 1, Table 4). The glass transition increases in line with the amount of GC. As expected, due to the generally atactic structure of the copolymers, amorphous materials were obtained and consequently no melting points were observed.

In **Figure 6**, the approximately linear relationships between the T_g of the acetal protected P(EEGE-*co*-GC) copolymers, the

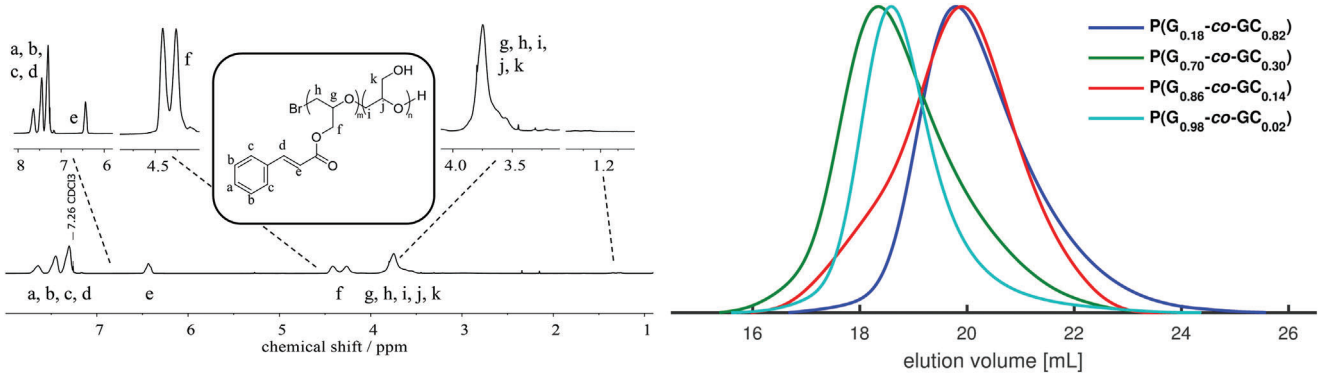

Figure 5. ^{1}H NMR spectrum (600 MHz, $CDCl_3$) of P($G_{0.18}$-*co*-$GC_{0.82}$) (entry 9, Table 3) and SEC traces (RI detector, DMF, PEG standards) of selected P(G-*co*-GC) copolymers.

Table 4. Thermal properties of P(EEGE-*co*-GC)/P(G-*co*-GC) copolymers and PGC homopolymer.

No.[a)]	Copolymer composition[b)]	T_g [°C]
1	PGC	21
2	P($EEGE_{0.17}$-*co*-$GC_{0.83}$)	8
3	P($EEGE_{0.27}$-*co*-$GC_{0.73}$)	−4
4	P($EEGE_{0.70}$-*co*-$GC_{0.30}$)	−42
5	P($EEGE_{0.81}$-*co*-$GC_{0.19}$)	−46
6	P($EEGE_{0.84}$-*co*-$GC_{0.16}$)	−53
7	P($EEGE_{0.92}$-*co*-$GC_{0.08}$)	−54
8	P($EEGE_{0.97}$-*co*-$GC_{0.03}$)	−60
9[(2)]	P($G_{0.18}$-co-$GC_{0.82}$)	16
10[(3)]	P($G_{0.29}$-co-$GC_{0.71}$)	16
11[(4)]	P($G_{0.70}$-co-$GC_{0.30}$)	9
12[(5)]	P($G_{0.81}$-co-$GC_{0.19}$)	1
13[(6)]	P($G_{0.86}$-co-$GC_{0.14}$)	−9
14[(7)]	P($G_{0.92}$-*co*-$GC_{0.08}$)	−16
15[(8)]	P($G_{0.98}$-co-$GC_{0.02}$)	−13

[a)] Exponent specifies precursor 2–8; [b)] Obtained from ^{1}H NMR spectra.

deprotected P(G-*co*-GC) copolymers and the PGC homopolymer are plotted as a function of their GC content. Please note that the T_gs of PEEGE and PG homopolymers were taken from literature and amount to −67[35] and −14 °C,[51] respectively. The T_gs of the copolymers are within these limits. The nearly linear trend for the P(EEGE-*co*-GC) copolymers demonstrates the effect of the incorporation of the comonomers EEGE and GC. However, the observed deviations can be derived from the gradient copolymer structure.

The systematic increase of the glass transition with rising GC content is due to the substituent effects. Bulky side chains, such as the sterically demanding cinnamic acid ester groups, impede mobility of the main chain and thus lead to an increase of the T_g.[52] Upon deprotection and release of the hydroxyl groups, a general increase of the T_gs in the series of P(G-*co*-GC) copolymers is observed ($\Delta T_{8\rightarrow15}$ = 47 °C), which is due to hydrogen bond interaction.[53] This effect becomes smaller with increasing GC content ($\Delta T_{2\rightarrow9}$ = 8 °C) demonstrating that the large, sterically demanding GC side groups possess a major impact on the glass transition of the respective samples.

For evaluation, the linear plot of the Fox Equation (1)[54] and the simple, linear combination based on the empirical Jenckel–Heusch Equation (2)[55] were used:

$$\frac{1}{T_g} = \frac{x_{EEGE/G}}{T_{g_{PEEGE/PG}}} + \frac{x_{GC}}{T_{g_{PGC}}} \quad (1)$$

$$T_g = x_{EEGE/G} \times T_{g_{PEEGE/PG}} + x_{GC} \times T_{g_{PGC}} \quad (2)$$

Here, x is the mole fraction of the monomer units EEGE/G and GC, whereas $T_{g_{PEEGE/PG}}$ and $T_{g_{PGC}}$ correspond to the respective homopolymer. These equations represent a simplified approach, which does not take specific interaction terms into account.[56] Direct comparison demonstrates that the measured T_g values for the protected P(EEGE-*co*-GC) copolymers agree reasonably well with the course of the Fox and modified Jenckel–Heusch equation. Thus, the glass transitions can be predicted for arbitrary P(EEGE-*co*-GC) copolymer compositions using these equations. For the deprotected P(G-*co*-GC) copolymers, a considerable deviation from the course of the fits is observed, which reaches its maximum at a composition of 40–50 mol% GC. This behavior can be attributed to the gradient copolymer structure as well as interactions and the considerations of the chemical nature of the comonomers.[57] As a consequence of hydrogen bonding between the ester function of GC and the hydroxyl groups of the glycerol moieties, higher T_gs are observed.[58]

2.6. Photocrosslinking of P(G-*co*-GC) Copolymers

Polyether copolymers with cinnamic acid functionality are promising for traceless photocrosslinking.[59a–d,60] The reactive double bond in the cinnamic acid side chain permits photodimerization and thus crosslinking of the copolymers, as shown in Figure S24, Supporting Information. In general, photocrosslinking of cinnamate derivatives requires UV radiation with $\lambda > 280$ nm (here 312 and 365 nm).[21,60,61] As a result, cinnamate units exhibit a substantial advantage, since no other reagents such as photoinitiators are required for crosslinking. The following section discusses the photodimerization-based crosslinking of the

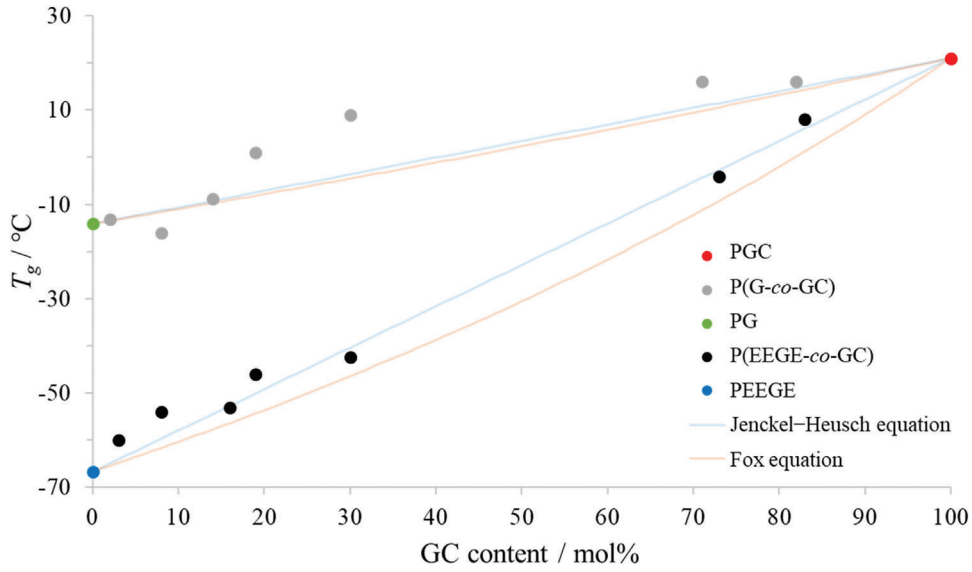

Figure 6. Glass transition temperatures of P(EEGE-*co*-GC)/P(G-*co*-GC) copolymers and PG/PEEGE/PGC homopolymers as a function of the GC content, including fits for the modified Jenckel–Heusch (blue curve) and Fox equation (red curve).

Table 5. Swelling behavior of the P(G-*co*-GC) hydrogels.

No.[a)]	Copolymer composition[b)]	*SR* [%]	Q_m
11[(4)]	P($G_{0.70}$-co-$GC_{0.30}$)	79	1.8
12[(5)]	P($G_{0.81}$-co-$GC_{0.19}$)	172	2.7
13[(6)]	P($G_{0.86}$-co-$GC_{0.14}$)	175	2.8
14[(7)]	P($G_{0.92}$-*co*-$GC_{0.08}$)	220	3.2
15[(8)]	P($G_{0.98}$-co-$GC_{0.02}$)	–	–

[a)] Exponent specifies precursor; [b)] Obtained from ^{1}H NMR spectra.

synthesized P(G-*co*-GC) copolymers in ethanol (14 wt%) by use of UV irradiation, allowing swelling of the crosslinked copolymer disks in water and formation of hydrogels.[62]

Direct crosslinking via photodimerization in aqueous solution failed, which might be attributed to the gradient-like microstructure of the copolymers that could lead to shielding of the less soluble glycidyl cinnamate units by the polar polyglycerol chains. A series of experiments was performed, varying both the concentration and UV irradiation times. Finally, the use of ethanol as a solvent turned out to be the best option as all P(G-*co*-GC) copolymers possessing a GC content below 30% were soluble. The copolymers were successfully photocrosslinked, and the solvent was allowed to evaporate slowly. For successful formation of hydrogels, the GC content in the copolymers must exceed 2 mol% (cf. entry 15, **Table 5**). After irradiation of the soft and adhesive ("sticky") starting material, a solid hydrogel was formed. Noticeable differences in the properties of the crosslinked copolymers were observed, depending on the amount of GC in the copolymers employed. While photocrosslinking of P($G_{0.92}$-*co*-$GC_{0.08}$) (entry 14, Table 3) resulted in an elastic material, crosslinked polymer films with higher amount of GC were quite brittle.

To confirm the successful photodimerization, IR spectroscopy was conducted as a qualitative method due to the insolubility of the crosslinked copolymers. Figure S25, Supporting Information, shows the superimposed, normalized IR spectra of the P(G-*co*-GC) copolymers after crosslinking. In particular, the wave number range of 1800 to 1600 cm^{-1} demonstrates successful crosslinking of the P(G-*co*-GC) copolymers. In the case of the non-crosslinked polymers, the unsaturated ester carbonyl band appears at $\nu_{C=O}$ = 1709 cm^{-1}, and the C=C stretching mode at $\nu_{C=C}$ = 1636 cm^{-1} (**Figure 7**). The IR spectrum shows a strong decrease of the C=C stretching mode after the photodimerization and a shift of the carbonyl band to 1731 cm^{-1}. According to Coleman et al., the difference between the unsaturated C=O and the saturated carbonyl stretching band is a consequence of the formation of saturated C–C crosslinks from the cinnamoyl double bonds (cf. Figure S24, Supporting Information).[63]

For the characterization of the hydrogels, the equilibrium swelling ratio (*SR*, Equation (3), see the Experimental Section) and mass swelling (Q_m, Equation (4), see the Experimental Section) in water were examined. Table 5 summarizes the *SR* and Q_m results for the P(G-*co*-GC) hydrogels.

The *SR* was calculated using Equation (3) and varies from 220% to 79%. However, the mass swelling (Equation (4)) decreases from 3.2 to 1.8, which is illustrated in Figure S26, Supporting Information. As expected, with increasing GC content, the water uptake decreases due to increasing crosslink density. The hydrogels exhibit rather low water uptake compared to PEG hydrogels.[64] This behavior is tentatively attributed to the microstructure of the P(G-*co*-GC) copolymers. According to the in-situ ^{1}H NMR kinetic measurements, the copolymer chains show a gradient-like distribution and consequently no uniformly distributed GC units. A large water uptake capacity requires rather long hydrophilic segments, leading to a large mesh size.[65] Instead, the crosslinks are concentrated in the GC-rich segments due to the gradient, resulting in a decreased mesh size and in reduced water uptake.[66]

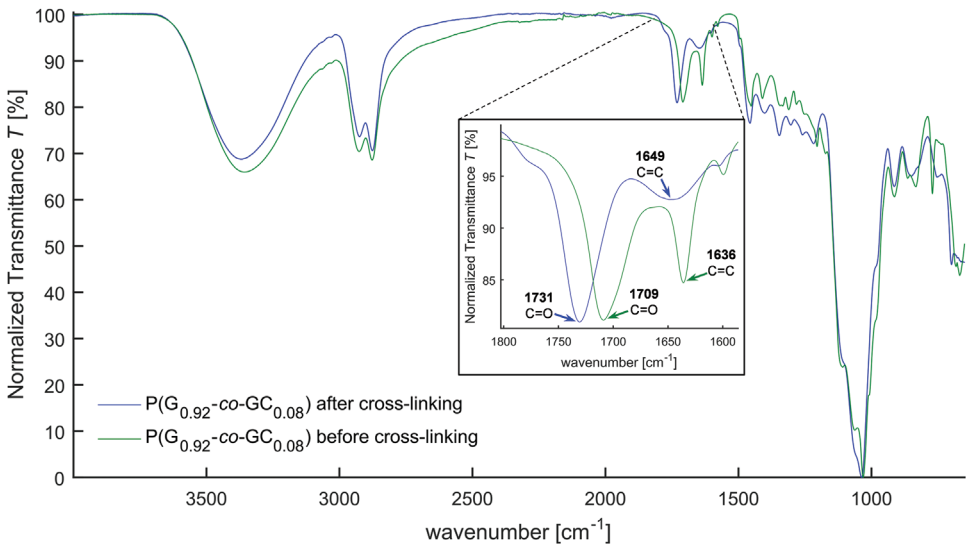

Figure 7. Normalized IR spectra of P($G_{0.92}$-*co*-$GC_{0.08}$) (entry 14, Table 3) before and after photocrosslinking, including a zoom-in of the GC double bond region.

3. Conclusion

By using the peculiar features of MAROP, the copolymerization of GC and EEGE has been introduced. Incorporation of the photoresponsive GC monomer in the biocompatible PG chains allows for the formation of cinnamoyl-crosslinked copolymer networks without additional photoinitiator and gives rise to promising candidates for biomedical applications. The results demonstrate that such reactive glycidyl esters, as a hardly studied class of epoxide monomers, are amenable to ring-opening polymerization reactions, if the monomer activation technique is employed. The amount of incorporated GC in the polymers varied from 3 mol% to 100 mol%, relying on an excess of triisobutylaluminum (*i*-Bu_3Al) as a catalyst in combination with tetraoctylammonium bromide ($NOct_4Br$) as an initiator. The obtained P(EEGE-*co*-GC) copolymers showed apparent molecular weights ranging from 2600 to 4600 g mol^{-1} with dispersities (*Đ*) below 1.34. Detailed characterization of the microstructure using insitu ^{1}H NMR kinetics revealed a gradient incorporation of the comonomers via the ideal copolymerization model ($r_{EEGE} = 0.28$; $r_{GC} = 3.6$). Density functional theory (DFT) calculations confirmed similar ring strain of GC and EO, for which a strong monomer gradient in the monomer-activated copolymerization with EEGE was recently demonstrated by our group.[39]

Selective cleavage of the acetal protecting groups, avoiding ester hydrolysis of the GC units, was achieved using Dowex ion exchange resin. The molecular weights of the resulting deprotected P(G-*co*-GC) copolymers varied from 1900 to 3700 g mol^{-1} while the dispersities *Đ* were in the range of 1.21 to 1.34. An investigation of the thermal properties demonstrated the effect of hydrogen bonds in the P(G-*co*-GC) copolymers. The glass transition temperatures (T_gs) ranged between −13 (deprotected polyethers) and −60 (protected polymer) to 21 °C for the PGC homopolymer. Photocrosslinking of the cinnamate-containing copolymers via UV irradiation enabled the formation of hydrogels with a water equilibrium swelling of up to 220%.

These characteristics render P(G-*co*-GC) copolymers interesting candidates for biomedical applications, particularly since the respective hydrogels are accessible without addition of initiators or crosslinking agents.[67] The results of this work may be of a general nature for the polymerization and copolymerization of the hitherto scarcely studied monomer class of glycidyl esters. By esterification of carboxylic acids with glycidol, a vast variety of different side chains is conveniently accessible, greatly enhancing the structural diversity of polyethers.

4. Experimental Section

Terminology: Linear polyglycerol is hereafter abbreviated as PG.

Instrumentation: ^{1}H NMR spectra (400 MHz or 600 MHz) were recorded on a Bruker Avance II 400 or Bruker Avance III 600 spectrometer. All spectra are referenced internally to residual proton signals of the deuterated solvent. In-situ ^{1}H NMR kinetics were measured on a Bruker Avance III HD 400 spectrometer equipped with a 5 mm BBFO SmartProbe (Z-gradient probe) and an ATM as well as a SampleXPress 60 auto sampler. SEC measurements were performed on an Agilent 1100 Series, equipped with a Polymer Standards Service (PSS) HEMA column (300/100/ 40 Å porosity), RI and UV (275 nm) detector. Dimethylformamide (containing 1 g L^{-1} of lithium bromide [LiBr]]) was used as a solvent at 50 °C and poly(ethylene glycol) standards provided by PSS were employed for calibration. All SEC samples were prepared in DMF (1 g L^{-1} LiBr) at a concentration of 1 mg L^{-1}. DSC measurements were performed on a Perkin Elmer 8500 with a temperature range of −80 to 80 °C, using heating and cooling rates of 20 (first cycle) and 10 °C min^{-1} (second cycle). For evaluation, the data points of the second heating cycle were used. IR spectra were recorded on a Nicolet iS10 Fourier transform infrared spectrometer (Thermo Fisher Scientific) with attenuated total reflection. Matrix-assisted Laser Desorption Ionization Time-of-Flight (MALDI-ToF) Mass Spectrometry was conducted on a Bruker MALDI-ToF MS Autoflex Max in the linear modulus. *Trans*-2-[3-(4-*tert*-Butylphenyl)-2-methyl-2-propenyliden]malononitrile (DCTB) and AgTFA were selected as matrix and salt additive, respectively.

DFT Calculations: Quantum mechanical calculations were carried out with the ORCA 3.0.2 software suite.[68] All structures were optimized using

the B3LYP DFT hybrid functional with geometrical counterpoise correction (gCP)[69] and dispersion correction (D3)[70] using def2-TZVP[71] as basis set and RIJK-COSX[72] as approximation. In all cases frequency analysis was performed and no imaginary frequency was detected.

Reagents: Chemicals and solvents were purchased from commercial suppliers (Acros, Sigma-Aldrich, Fisher Scientific, Alfa Aesar) and used without prior purification, unless otherwise stated. Deuterated solvents were obtained from Deutero GmbH. *i*-Bu_3Al (1.1 M solution in toluene, Acros Organics) and toluene (99.85%, Acros Organics) were used without further purification. $NOct_4Br$ (98%, TCI) was azeotropically dried with benzene overnight under reduced pressure. GC was purified by stirring over CaH_2 and distillation. EEGE was synthesized according to Fitton et al.[27] and dried analogously. Dialysis membranes (regenerated cellulose, MWCO = 1000 g mol^{-1}) were obtained from Orange Scientific.

Monomer Synthesis (Glycidyl Cinnamate: GC was prepared in a two-step synthesis. For the preparation of potassium cinnamate (PC), cinnamic acid (2 g, 13 mmol, 1 equiv.) was dissolved in THF (20 mL) in a round-bottom flask and heated to 30 °C. While stirring, freshly ground potassium hydroxide (0.8 g, 13 mmol, 1 equiv.) was added to the reaction solution. After one hour, the solvent was removed in vacuo. Yield: quantitative.

The second reaction step was performed according to a slightly modified procedure of Rusu et al.[14] PC (1.5 g, 8 mmol, 1.0 equiv.) and epichlorohydrin (7.9 mL, 101 mmol, 12.5 equiv.) were placed in a reaction flask. Subsequently, tetrabutylammonium bromide (130 mg, 0.4 mmol, 0.05 equiv.) was added and the reaction mixture was stirred at reflux of 115 °C for 3.5 h. The clear orange solution was diluted with dichloromethane (40 mL) and potassium chloride was filtered off. After washing twice with a saturated, aqueous $NaHCO_3$ solution (100 mL), the organic phase was dried over $MgSO_4$ and concentrated using a rotary evaporator. By distillation of the orange solution under reduced pressure, the product was isolated as a colorless, viscous liquid. Yield: 85%.

^{1}H NMR (400 MHz, $CDCl_3$): δ (ppm) = 2.67 (dd, 1H, H_a), 2.84 (t, 1H, H_a), 3.26 (m, 1H, H_b), 4.02 (dd, 1H, H_c), 4.53 (dd, 1H, H_c), 6.45 (d, 1H, H_d), 7.35 (m, 3H, H_f, H_h), 7.50 (m, 2H, H_g), 7.71 (d, 1H, H_e). ^{13}C NMR (100 MHz, $CDCl_3$): δ (ppm) = 44.64 (C_a), 49.43 (C_b), 65.04 (C_c), 117.30 (C_e), 128.11 (C_i), 128.88 (C_h), 130.44 (C_j), 134.16 (C_g), 145.50 (C_f), 166.49 (C_d).

Copolymerization of EEGE and GC: The following protocol was performed in analogy to the literature procedure for the polymerization of EEGE according to Carlotti and Deffieux[9] and refers to the sample P($EEGE_{0.17}$-*co*-$GC_{0.83}$) (entry 2, Table 1, ($M_n^{(th)}$) of 10 000 g mol^{-1}, theoretical molar composition of EEGE:GC = 19:81). Tetraoctylammonium bromide (0.1 g, 0.09 mmol, 1 equiv.) was freeze-dried with benzene (3 mL) in a Schlenk tube. Anhydrous toluene (5 mL) and the dried monomers GC (0.7 mL, 3.84 mmol, 42 equiv.) and EEGE (0.1 mL, 0.91 mmol, 10 equiv.) were added to the initiator via syringe under argon atmosphere. After cooling to −72 °C with an ethanol/dry ice bath, the polymerization was initiated by injection of the catalyst *i*-Bu_3Al (0.4 mL, 0.41 mmol, 4.5 equiv.), resulting in a strong yellow color that decreased during the reaction. The reaction mixture was slowly warmed to room temperature. Termination was carried out after 48 h by addition of Milli-Q water (1 mL). $Al(OH)_3$ precipitated as a white solid, which was removed by filtration. The polymer solution was concentrated in vacuo. For purification the copolymer was dissolved in dichloromethane and dialyzed against dichloromethane/methanol (3:2) for 24 h. Drying under vacuum afforded the copolymer in yields of 90%.

^{1}H NMR (600 MHz, $CDCl_3$): δ (ppm) = 1.15 (br, H_o), 1.22 (br, H_l), 3.36–4.01 (br, H_g, H_h, H_i, H_j, H_k, H_n), 4.32 (br, H_f), 4.70 (s, H_m), 6.43 (br, H_e), 7.30–7.45 (br, H_a, H_b, H_c), 7.64 (br, H_d). ^{13}C NMR (150 MHz, $CDCl_3$): δ (ppm) = 15.28 (C_q), 19.80 (C_n), 60.99 (C_p), 63.71 (C_h, C_j, C_l), 69.51 (C_m), 77.74 (C_i, C_k), 99.81 (C_o), 117.69 (C_f), 128.17–128.85 (C_b, C_c), 130.33 (C_a), 134.25 (C_d), 145.20 (C_e), 166.69 (C_g).

Deprotection of P(EEGE-co-GC): Removal of the acetal protecting group under acidic conditions was performed using the ion exchange resin Dowex 50WX8. For this purpose, the copolymer was dissolved in a methanol/toluene mixture (2:1, 20 wt%) to which Dowex was added. In order to shift the reaction equilibrium, the volatile by-products (acetaldehyde and ethanol) were removed under reduced pressure at 30 °C for 12 h. The resin residue was filtered before the polymer was dried in vacuo. Yield: 90% to quantitative.

^{1}H NMR (600 MHz, $CDCl_3$): δ (ppm) = 3.48–3.97 (br, H_g, H_h, H_i, H_j, H_k), 4.34 (br, H_f), 6.43 (br, H_e), 7.30–7.45 (br, H_a, H_b, H_c), 7.60 (br, H_d). ^{13}C NMR (150 MHz, $CDCl_3$): δ (ppm) = 63.62 (C_h, C_j, C_l), 69.72 (C_m), 77.74 (C_i, C_k), 117.61 (C_f), 128.21–128.91 (C_b, C_c), 130.37 (C_a), 134.22 (C_d), 145.28 (C_e), 166.75 (C_g).

In-Situ ^{1}H NMR Kinetic Studies: In the first step the initiator tetraoctylammonium bromide ($NOct_4Br$, 50 mg) was dried in a Schlenk tube by dissolving it in 2 mL benzene and stirring under vacuum for 30 min at 60 °C. After removing the solvent under vacuum for 24 h, 0.5 mL dry toluene-d_8 were added. A Norell S-5-400-VT-7 NMR tube was evacuated overnight and filled with argon. 0.1 mL of the initiator solution ($NOct_4Br$, 1 equiv.) was added in the NMR tube, followed by 0.55 mL toluene-d_8. Glycidyl cinnamate (GC) and EEGE were dried over CaH_2 and distilled under reduced pressure. 47 µL GC (15 equiv.) and 40 µL EEGE (15 equiv.) were placed in the NMR tube. After cooling with an acetone/dry ice bath for 20 min, 83 µL *i*-Bu_3Al solution (1.1 M in toluene, 5 equiv.) was injected via syringe. The NMR tube was sealed with a Teflon stop-cock and shaken vigorously in order to homogenize the solution before placing the tube in the NMR spectrometer with the probe gas flow adjusted to −20 °C. When a stable temperature in the probe head was reached (≈10 min, ΔT = 0.1 K), the first spectrum was recorded. Sample spinning was turned off. Spectra were recorded with 16 scans at 2 min intervals throughout the entire measurement. The measurement was stopped at full conversion (≈2 h). SEC data of the isolated P($EEGE_{0.50}$-*co*-$GC_{0.50}$) copolymer is shown in Figure S13, Supporting Information.

Crosslinking by UV Irradiation and Study of Swelling Behavior: Crosslinking experiments were performed in small PTFE pans (ϕ = 20 mm). For this purpose, an ethanolic P(G-*co*-GC) solution (c = 140 g L^{-1}) was transferred into the pans. The pans were covered with a quartz glass slide in order to avoid contamination and rapid evaporation of the solvent. For the irradiation, a UV lamp was used, into which UV tubes with wavelengths of 312 nm and 364 nm were installed. After 180 min, the crosslinked copolymer films were removed from the pans.

For the study of the swelling properties, the hydrogels were placed in Milli-Q water for 48 h in order to reach equilibrium swelling. Subsequently, the swollen hydrogels were removed and weighed after removal surface adsorbed water by Kimwipes. The hydrogels were allowed to swell in water again for 1 h and the process was repeated three times to determine the standard deviation. Swelling ratio (*SR*) was determined using the following expression:[73]

$$WSR = \left(\frac{w_s - w_d}{w_d}\right) \times 100 \quad (3)$$

where w_s and w_d are the weights of the swollen and dry hydrogels, respectively. The mass swelling (Q_m) was calculated according to:[73]

$$Q_m = \frac{w_s}{w_d} \quad (4)$$

Supporting Information

Supporting Information is available from the Wiley Online Library or from the author.

Acknowledgements

K.M. and S.S. contributed equally to this work. The authors thank Nadine Schenk for technical assistance. J.B. acknowledges the Graduate School of Excellence MAINZ for financial support. T.J. thanks the MPGC Mainz and the Gutenberg Academy for financial support.

Open access funding enabled and organized by Projekt DEAL.

Conflict of Interest

The authors declare no conflict of interest.

Data Availability Statement

The data that support the findings of this study are available on request from the corresponding author. The data are not publicly available due to privacy or ethical restrictions.

Keywords

ethoxyethyl glycidyl ether, glycidyl cinnamate, hydrogels, in-situ ^{1}H NMR kinetics , monomer-activated polymerization, photocrosslinking, polyglycerol

Received: October 7, 2022
Revised: November 1, 2022
Published online: November 24, 2022

[1] a) K. Matyjaszewski, N. V. Tsarevsky, *Nat. Chem.* **2009**, *1*, 276; b) V. Coessens, T. Pintauer, K. Matyjaszewski, *Prog. Polym. Sci.* **2001**, *26*, 337; c) M. Ouchi, T. Terashima, M. Sawamoto, *Chem. Rev.* **2009**, *109*, 4963.
[2] C. P. Kabb, C. S. O'Bryan, C. C. Deng, T. E. Angelini, B. S. Sumerlin, *ACS Appl. Mater. Interfaces* **2018**, *10*, 16793.
[3] a) R. A. El-Ghazawy, A. M. El-Saeed, H. I. Al-Shafey, A.-R. M. Abdul-Raheim, M. A. El-Sockary, *Eur. Polym. J.* **2015**, *69*, 403; b) K. Huang, Z. Liu, J. Zhang, S. Li, M. Li, J. Xia, Y. Zhou, *Biomacromolecules* **2014**, *15*, 837; c) H. Yu, L. Wang, J. Huo, J. Ding, Q. Tan, *J. Appl. Polym. Sci.* **2008**, *110*, 1594; d) A. M. Atta, R. Mansour, M. I. Abdou, A. M. Sayed, *Polym. Adv. Technol.* **2004**, *15*, 514; e) P.-A. Martínez, V. Cádiz, A. Serra, A. Mantecón, *Angew. Makromol. Chem.* **1985**, *136*, 159.
[4] a) J. Herzberger, K. Niederer, H. Pohlit, J. Seiwert, M. Worm, F. R. Wurm, H. Frey, *Chem. Rev.* **2016**, *116*, 2170; b) H. Staudinger, H. Lohmann, *Justus Liebigs Ann. Chem.* **1933**, *505*, 41.
[5] C. Billouard, S. Carlotti, P. Desbois, A. Deffieux, *Macromol. Chem. (Oxford)* **2004**, *37*, 4038.
[6] A. Labbé, S. Carlotti, C. Billouard, P. Desbois, A. Deffieux, *Macromol. Chem. (Oxford)* **2007**, *40*, 7842.
[7] a) A.-L. Brocas, C. Mantzaridis, D. Tunc, S. Carlotti, *Prog. Polym. Sci.* **2013**, *38*, 845; b) S. Carlotti, A. Labbé, V. Rejsek, S. Doutaz, M. Gervais, A. Deffieux, *Macromol. Chem. (Oxford)* **2008**, *41*, 7058; c) E. Cevada, K. Roos, F. Alvarez, S. Carlotti, F. Vázquez, *Fuel* **2018**, *221*, 447.
[8] M. Gervais, A.-L. Brocas, A. Deffieux, E. Ibarboure, S. Carlotti, *Pure Appl. Chem.* **2012**, *84*, 2103.
[9] M. Gervais, A.-L. Brocas, G. Cendejas, A. Deffieux, S. Carlotti, *Macromol. Chem. (Oxford)* **2010**, *43*, 1778.
[10] A. Labbé, A.-L. Brocas, E. Ibarboure, T. Ishizone, A. Hirao, A. Deffieux, S. Carlotti, *Macromol. Chem. (Oxford)* **2011**, *44*, 6356.
[11] O. Linker, J. Blankenburg, K. Maciol, M. Bros, H. Frey, *Macromolecules* **2020**, *53*, 3524.
[12] G. Kwon, M. Kim, W. H. Jung, S. Park, T.-T. H. Tam, S.-H. Oh, S.-H. Choi, D. J. Ahn, S.-H. Lee, B.-S. Kim, *Macromolecules* **2021**, *54*, 8478.
[13] H. Shen, J. Chen, M. Taha, *Polym. J.* **2014**, *46*, 598.
[14] E. Rusu, E. Comanita, A. Airinei, G. Rusu, *Iran. Polym. J.* **1998**, *7*, 157.
[15] T. Nishikubo, T. Ichijyo, T. Takaoka, *Nippon Kagaku Kaishi* **1973**, *10*, 1851.
[16] S. Fadlallah, P. Sinha Roy, G. Garnier, K. Saito, F. Allais, *Green Chem.* **2021**, *23*, 1495.
[17] a) S.-J. Sung, K.-Y. Cho, H. Hah, J. Lee, H.-K. Shim, J.-K. Park, *Polymer* **2006**, *47*, 2314; b) D. Creed, A. C. Griffin, C. E. Hoyle, K. Venkataram, *J. Am. Chem. Soc.* **1990**, *112*, 4049; c) S. Chatani, C. J. Kloxin, C. N. Bowman, *Polym. Chem.* **2014**, *5*, 2187.
[18] P. L. Egerton, E. Pitts, A. Reiser, *Macromol. Chem. (Oxford)* **1981**, *14*, 95.
[19] M. Jamróz-Piegza, W. Wałach, A. Dworak, B. Trzebicka, *J. Colloid Interface Sci.* **2008**, *325*, 141.
[20] S. Murase, K. Kinoshita, K. Horie, S. Morino, *Macromol. Chem. (Oxford)* **1997**, *30*, 8088.
[21] K. Ichimura, Y. Akita, H. Akiyama, K. Kudo, Y. Hayashi, *Macromol. Chem. (Oxford)* **1997**, *30*, 903.
[22] D. Shi, M. Matsusaki, M. Akashi, *J. Controlled Release* **2011**, *149*, 182.
[23] X. Zhao, P. Shan, H. Liu, D. Li, P. Cai, Z. Li, Z. Li, *Front. Chem.* **2020**, *8*, 839.
[24] a) A. Thomas, S. S. Müller, H. Frey, *Biomacromolecules* **2014**, *15*, 1935; b) A. Dworak, S. Slomkowski, T. Basinska, M. Gosecka, W. Walach, B. Trzebicka, *Polimery* **2013**, *58*, 641.
[25] H. Keul, M. Möller, *J. Polym. Sci. A Polym. Chem* **2009**, *47*, 3209.
[26] D. Wilms, S.-E. Stiriba, H. Frey, *Acc. Chem. Res.* **2010**, *43*, 129.
[27] A. O. Fitton, J. Hill, D. E. Jane, R. Millar, *Synthesis* **1987**, *1987*, 1140.
[28] a) S. Halacheva, S. Rangelov, C. Tsvetanov, *Macromol. Chem. (Oxford)* **2006**, *39*, 6845; b) P. Dimitrov, St. Rangelov, A. Dworak, N. Haraguchi, A. Hirao, C. Tsvetanov, *Macromol. Symp.* **2004**, *215*, 127; c) F. Wurm, J. Nieberle, H. Frey, *Macromolecules* **2008**, *41*, 1184; d) C. Mangold, F. Wurm, B. Obermeier, H. Frey, *Macromol. Rapid Commun.* **2010**, *31*, 258; e) D. Taton, A. Le Borgne, M. Sepulchre, N. Spassky, *Macromol. Chem. Phys.* **1994**, *195*, 139; f) J. Blankenburg, K. Maciol, C. Hahn, H. Frey, *Macromolecules* **2019**, *52*, 1785.
[29] Z. Li, Y. Chau, *Bioconjugate Chem.* **2009**, *20*, 780.
[30] F. Wurm, C. Dingels, H. Frey, H.-A. Klok, *Biomacromolecules* **2012**, *13*, 1161.
[31] a) M. Weinhart, I. Grunwald, M. Wyszogrodzka, L. Gaetjen, A. Hartwig, R. Haag, *Chem. - Asian J.* **2010**, *5*, 1992; b) M. Weinhart, T. Becherer, R. Haag, *Chem. Commun.* **2011**, *47*, 1553.
[32] M. Hans, P. Gasteier, H. Keul, M. Moeller, *Macromolecules* **2006**, *39*, 3184.
[33] M. Hans, H. Keul, M. Moeller, *Polymer* **2009**, *50*, 1103.
[34] a) J. Meyer, H. Keul, M. Möller, *Macromol. Chem. (Oxford)* **2011**, *44*, 4082; b) S. S. Müller, C. Moers, H. Frey, *Macromolecules* **2014**, *47*, 5492.
[35] M. Schömer, H. Frey, *Macromol. Chem. (Oxford)* **2012**, *45*, 3039.
[36] D. C. Schriemer, L. Li, *Anal. Chem.* **1997**, *69*, 4169.
[37] J. Herzberger, H. Frey, *Macromol. Chem. (Oxford)* **2015**, *48*, 8144.
[38] V. Rejsek, D. Sauvanier, C. Billouard, P. Desbois, A. Deffieux, S. Carlotti, *Macromol. Chem. (Oxford)* **2007**, *40*, 6510.
[39] J. Herzberger, D. Leibig, J. C. Liermann, H. Frey, *ACS Macro Lett.* **2016**, *5*, 1206.
[40] C. Schubert, P. Dreier, T. Nguyen, K. Maciol, J. Blankenburg, C. Friedrich, H. Frey, *Kobunja Kwahak Kwa Kisul* **2017**, *121*, 328.
[41] B. Obermeier, F. Wurm, H. Frey, *Macromol. Chem. (Oxford)* **2010**, *43*, 2244.
[42] S. Heinen, S. Rackow, A. Schäfer, M. Weinhart, *Macromol. Chem. (Oxford)* **2017**, *50*, 44.
[43] F. Heatley, G.-E. Yu, C. Booth, T. G. Blease, *Eur. Polym. J.* **1991**, *27*, 573.
[44] J. Blankenburg, E. Kersten, K. Maciol, M. Wagner, S. Zarbakhsh, H. Frey, *Polym. Chem.* **2019**, *10*, 2863.
[45] F. T. Wall, *J. Am. Chem. Soc.* **1941**, *63*, 1862.
[46] V. Jaacks, *Makromol. Chem.* **1972**, *161*, 161.
[47] F. R. Mayo, F. M. Lewis, *J. Am. Chem. Soc.* **1944**, *66*, 1594.
[48] V. E. Meyer, G. G. Lowry, *J. Polym. Sci., Part A: Gen. Pap.* **1965**, *3*, 2843.
[49] C. Wahlen, J. Blankenburg, P. von Tiedemann, J. Ewald, P. Sajkiewicz, A. H. E. Müller, G. Floudas, H. Frey, *Macromolecules* **2020**, *53*, 10397.

[50] I. Skeist, *J. Am. Chem. Soc.* **1946**, *68*, 1781.
[51] C. Osterwinter, C. Schubert, C. Tonhauser, D. Wilms, H. Frey, C. Friedrich, *Macromol. Chem. (Oxford)* **2015**, *48*, 119.
[52] A. Singh, N. R. Krogman, S. Sethuraman, L. S. Nair, J. L. Sturgeon, P. W. Brown, C. T. Laurencin, H. R. Allcock, *Biomacromolecules* **2006**, *7*, 914.
[53] C. Moers, R. Wrazidlo, A. Natalello, I. Netz, M. Mondeshki, H. Frey, *Macromol. Rapid Commun.* **2014**, *35*, 1075.
[54] T. G. Fox, *Bull. Am. Phys. Soc.* **1956**, *1*, 123.
[55] E. Jenckel, R. Heusch, *Kolloid-Z.* **1953**, *130*, 89.
[56] T. K. Kwei, *J. Polym. Sci., Polym. Lett. Ed.* **1984**, *22*, 307.
[57] R. París, J. L. de La Fuente, *J. Polym. Sci. B Polym. Phys.* **2007**, *45*, 1845.
[58] a) A. Sanchis, M. G. Prolongo, R. G. Rubio, R. M. Masegosa, *Polym. J.* **1995**, *27*, 10; b) A. Sanchis, M. G. Prolongo, C. Salom, R. M. Masegosa, *J. Polym. Sci. B Polym. Phys.* **1998**, *36*, 95.
[59] a) Y. Ni, S. Zheng, *Chem. Mater.* **2004**, *16*, 5141; b) I. Assaid, D. Bosc, I. Hardy, *J. Phys. Chem. B* **2004**, *108*, 2801; c) A. Guo, G. Liu, J. Tao, *Macromol. Chem. (Oxford)* **1996**, *29*, 2487; d) L. Fertier, H. Koleilat, M. Stemmelen, O. Giani, C. Joly-Duhamel, V. Lapinte, J.-J. Robin, *Prog. Polym. Sci.* **2013**, *38*, 932.
[60] P. Gupta, S. R. Trenor, T. E. Long, G. L. Wilkes, *Macromolecules* **2004**, *37*, 9211.
[61] D. Shi, M. Matsusaki, T. Kaneko, M. Akashi, *Macromol. Chem. (Oxford)* **2008**, *41*, 8167.
[62] a) Q. Z. Yang, C. J. Fan, X. G. Yang, L. Q. Liao, L. J. Liu, *J. Appl. Polym. Sci.* **2016**, *133*, 43451; b) S. Salehpour, C. J. Zuliani, M. A. Dubé, *Eur. J. Lipid Sci. Technol.* **2012**, *114*, 92.
[63] M. M. Coleman, Y. Hu, M. Sobkowiak, P. C. Painter, *J. Polym. Sci. B Polym. Phys.* **1998**, *36*, 1579.
[64] a) K. Niederer, C. Schüll, D. Leibig, T. Johann, H. Frey, *Macromolecules* **2016**, *49*, 1655; b) I. Molina, S. Li, M. B. Martinez, M. Vert, *Biomaterials* **2001**, *22*, 363; c) S. Kaga, S. Yapar, E. M. Gecici, R. Sanyal, *Macromol. Chem. (Oxford)* **2015**, *48*, 5106; d) D. Cohn, T. Stern, M. F. González, J. Epstein, *J. Biomed. Mater. Res.* **2002**, *59*, 273.
[65] S. J. Bryant, R. J. Bender, K. L. Durand, K. S. Anseth, *Biotechnol. Bioeng.* **2004**, *86*, 747.
[66] J. Berger, M. Reist, J. M. Mayer, O. Felt, N. A. Peppas, R. Gurny, *Eur. J. Pharm. Biopharm.* **2004**, *57*, 19.
[67] T. R. Hoare, D. S. Kohane, *Polymer* **2008**, *49*, 1993.
[68] F. Neese, *Wiley Interdiscip. Rev.: Comput. Mol. Sci.* **2012**, *2*, 73.
[69] H. Kruse, S. Grimme, *J. Chem. Phys.* **2012**, *136*, 154101.
[70] a) S. Grimme, S. Ehrlich, L. Goerigk, *J. Comput. Chem.* **2011**, *32*, 1456; b) S. Grimme, J. Antony, S. Ehrlich, H. Krieg, *J. Chem. Phys.* **2010**, *132*, 154104.
[71] a) A. Schäfer, H. Horn, R. Ahlrichs, *J. Chem. Phys.* **1992**, *97*, 2571; b) F. Weigend, R. Ahlrichs, *Phys. Chem. Chem. Phys.* **2005**, *7*, 3297.
[72] F. Neese, F. Wennmohs, A. Hansen, U. Becker, *Chem. Phys.* **2009**, *356*, 98.
[73] M. Peter, P. Tayalia, *RSC Adv.* **2016**, *6*, 40878.

